Molecular Crystals and Liquid Crystals

ISSN: 1542-1406 (Print) 1563-5287 (Online) Journal homepage: http://www.tandfonline.com/loi/gmcl20

Production and Study of Silver Nanoparticles by 532 nm Laser Pulse Ablation in NaCl Solution

N. S. Andarkhor & D. Dorranian

To cite this article: N. S. Andarkhor & D. Dorranian (2014) Production and Study of Silver Nanoparticles by 532 nm Laser Pulse Ablation in NaCl Solution, Molecular Crystals and Liquid Crystals, 605:1, 12-22, DOI: 10.1080/15421406.2014.881695

To link to this article: http://dx.doi.org/10.1080/15421406.2014.881695

Published online: 15 Dec 2014.

Mol. Cryst. Liq. Cryst., Vol. 605: pp. 12–22, 2014

ISSN: 1542-1406 print/1563-5287 online
DOI: 10.1080/15421406.2014.881695

Production and Study of Silver Nanoparticles by 532 nm Laser Pulse Ablation in NaCl Solution

N. S. ANDARKHOR[1,*] AND D. DORRANIAN[2]

[1]Department of Physics, Science Faculty, Central Tehran Branch, Islamic Azad University, Tehran, Iran
[2]Laser Lab., Plasma Physics Research Center, Science and Research Branch, Islamic Azad University, Tehran, Iran

In this experimental research, silver nanoparticles are produced in NaCl solution by the laser ablation method. Our aim was to investigate the effect of the amount of NaCl in the ablation medium on the characteristics of nanoparticles. A 7 ns pulsed Neodymium YAG laser (Nd:YAG) at 5 J/cm2 fluence and 532 nm wavelength was employed to produce Ag nanoparticles in distilled water with four different concentrations of NaCl. The optical properties, size distribution, and agglomeration of nanoparticles were investigated by several diagnostics. The UV–Visible absorption spectra of the Ag nanoparticles exhibit absorptions in the UV region because of surface plasmon resonance. Transmission electron microscopy (TEM) and scanning electron microscopy (SEM) were used to study the size distribution and morphology of nanoparticles. Dynamic light scattering (DLS) was employed to measure the hydrodynamic size of nanoparticles in suspensions. With X-ray diffraction (XRD) pattern, the lattice structure of nanoparticles was studied. Fourier transform infrared (FTIR), photoluminescence (PL) spectra were obtained to observe the molecular structure and atomic energy levels of particles.

Keywords Absorption spectra; neodymium YAG laser; pulsed laser ablation (PLA); SEM; silver nanoparticles; TEM; XRD

Introduction

The determination of particle size in the nano region has been a subject of increasing interest during recent years. Among the diverse fields of applied sciences that involve this subject, the studies of atmospheric and combustion aerosols, the analysis of interstellar dust, and the characterization of many biological, chemical, and physical systems of interest for industrial processes stand out. Materials science is another field of interest where it is recognized that many properties of materials are affected by the size and characteristics of the particles within them. To understand the influence of particles in nature or to control industrial processes involving them, it is essential to develop methods to measure their size [1]. These particles are under active research because they possess interesting physical properties differing considerably from that of the bulk phase. It comes from small sizes and

*Address correspondence to N. S. Andarkhor, Department of Physics, Science Faculty, Central Tehran Branch, Islamic Azad University, Tehran, Iran. Tel: +98 21 44869654; Fax: +98 21 44869640. E-mail: naemeh.andarkhor@gmail.com

Color versions of one or more of the figures in the article can be found online at www.tandfonline.com/gmcl.

high surface/volume ratio [2]. The size-dependent unique physical and chemical properties of metal nanoparticles have many useful applications as in catalysis [3–5], biotechnology [6–8], and micro- or nanowiring [9–11]. Among them, silver (Ag) nanoparticles are one of the most popular catalysts for oxidation of ethylene and have higher electrical and thermal conductvities than other nanoparticles [12]. Silver nanoparticles are proven to be more effective as they have good antimicrobial efficacy against bacteria, viruses, and other eukaryotic micro-organisms [13]. The current investigations support that use of silver ion or metallic silver as well as silver nanoparticles can be exploited in medicine for burn treatment, dental materials, coating stainless steel materials, textile fabrics, water treatment, sunscreen lotions, etc. and possess low toxicity to human cells, high thermal stability, and low volatility [14]. Engineered nanoparticles are used in biomedical applications such as antibacterial implants or catheters and for modification of textiles and refinement of polymers [15]. Silver nanoparticles are also used in biosensors for glucose monitoring in diabetes patients and other medical health-related targets. The synthesis of metal nanoparticles is a subject of current interest due to their unique properties and promising applications [16]. Silver nanoparticles can be synthesized using various methods: chemical, electrochemical [17], γ-radiation [18], photochemical [19], laser ablation [20] etc. Among others, the pulsed laser ablation (PLA) method has been attracting much interest for producing organic nanoparticles [21]. Pulsed laser ablation in liquid media of a solid target has been proven to provide an efficient approach for preparing various nanoscale materials [22]. Material can be removed from the target if the excitation energy from the laser irradiation is above the ablation threshold. The removed material will relax (condense) back to the solid phase. The ablation of noble metals, such as gold and silver, in solvents, such as water, ethanol, and *n*-hexane results mainly in metallic particles. The size control of the noble metal nanoparticles fabricated by laser ablation could be achieved by adding specific molecules to the aqueous fabrication environment, which physically or chemically interact with the surfaces of the forming particles, to limit their growth. The structure and size of the resulting solid phase material after condensation can be controlled by the experimental conditions, for example, laser wavelength, intensity, pulse duration, environment temperature, and pressure [23].

In this study, we have focused on fabrication and characterization of the Ag nanoparticles in the NaCl solution by pulsed laser ablation of a silver target in the solution. We also explore the effect of NaCl amount in the ablation medium on the characteristics of nanoparticles at room temperature. The presence of chlorides in the aqueous medium during laser ablation turned out to provide reduction of the average particle size, prevent formation of large particles, and increase the formation efficiency of small nanoparticles thereby. However, the long-term stability of Ag nanoparticles formed in NaCl solution was reduced by enhanced spontaneous aggregation compared to those in distilled water.

The paper is organized as follows; following the introduction in Section 1, the experimental setup is presented in Section 2. Section 3 is devoted to results and discussions and Section 4 includes conclusion.

Experimental Setup

Silver nanoparticles were produced by pulsed laser ablation (PLA) of an Ag plate (99.9%) in NaCl solution. The Ag plate was cleaned ultrasonically in alcohol, acetone, and deionized water before the experiments. Nanoparticles were prepared using the second harmonics of an Nd:YAG laser operating at 532 nm. Laser pulsed width was of 7 ns with a 2 Hz repetition rate. Pure silver target was ablated for 8 min at laser fluence of 5 J/cm^2. The laser beam of 6 mm in diameter was focused using a lens with a focal length of 80 mm, exactly onto the

surface of the target. Height of water on the silver target was 1.2 cm. Laser beam diameter was 6 mm before lens and was calculated to be about 40 μm on the surface of the target. The volume of the solution in the ablation container was 30 ml and silver target was ablated with 1000 laser pulses at laser fluences. Samples 1–4 were prepared with concentration of NaCl solution 0, 5, 10, and 15 mM, respectively.

A variety of analytical techniques were applied for the characterization of products. For optical absorption spectra of samples in a 10 mm path length, quartz cells were measured by UV–Vis-NIR spectrophotometer from PG Instruments (T-80). Dynamic Light Scattering (DLS) device measurement was done using the Nano Zetasizer HSA 3000 device from English Malvern Co. for studying the hydrodynamic size distribution of the nanoparticles in NaCl solutions. Normally, 100 or more particles were counted to determine the size distribution of each sample. Transmission electron microscopy (TEM, Zeiss-EM10C-80KV) was conducted by placing a drop of the concentrated suspension on a carbon-coated copper grid. To further confirm the morphology of nanoparticles produced by pulsed laser ablation in NaCl solution, we performed Scanning electron microscopy (SEM, KYKY-EM3200) analysis. X-ray diffraction was measured, and with XRD pattern the lattice structure of nanoparticles was studied. Room temperature photoluminescence (PL, Luminescence Spectrometer- Ls-5) device from USA PERKIN ELMER Co. was used to characterize the samples to study the luminescence properties of the nanoparticles.

To measure the ablation rate in the liquid medium, the target was weighed up before and after the ablation process by Sartorius Utensil model CP225D with 0.01 mg readability. After ablation inside NaCl solution with 1000 laser pulses, the target was dried and weighed up again. Hence, the mass loss of the target is attributed to the amount of generated nanoparticles.

Results and Discussion

In Fig. 1, the photographs of samples are presented and in Table 1 the ablation rate of samples for concentration of NaCl in solution is shown. Depending on nanoparticle size and concentration, the color of silver nanoparticle solution for different samples is shown similar to that shown in Fig. 1. One reason can be due to the amount of nanoparticles in the

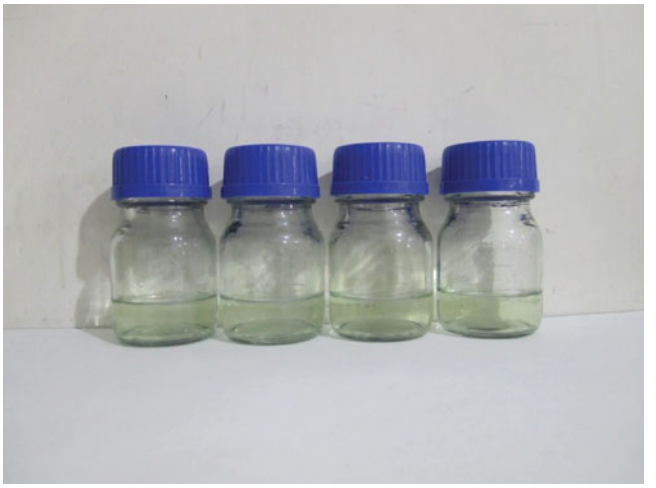

Figure 1. Ag nanoparticle samples in NaCl solution.

Table 1. Ablation mass rate of the target (1000 pulls)

Sample number	1	2	3	4
Mass range measured before and after the process of laser ablation (gr)	[10.6207–10.6206]	[10.6206–10.6205]	[10.6205–10.6203]	[10.6203–10.6202]
Removed mass during the process of laser ablation (gr)	0.0001	0.0001	0.0002	0.0001

NaCl solution. In Table 1, it is shown that the amount of silver nanoparticles is ablated by a small amount on increasing the concentration of NaCl in solution.

The structure of the laser-produced particles was characterized by XRD, so that the crystallite phase and purity of as-synthesized nanowires are ascertained using this method and the corresponding XRD pattern is shown in Fig. 2. The XRD pattern shows that the face-centered cubic phase and hexagonal phase of Ag coexist. Figure 2 shows the X-ray diffraction patterns of nanoparticles obtained by PLA of an Ag plate in different-concentration NaCl solutions; The peaks can be indexed into the cubic phase of NaCl, Ag_2O, and AgCl,Ag. It was observed that the characteristic sharp symmetric peak for the silver nanoparticle appeared at 2θ angles of 38° and 44° corresponding to the (111), (200) crystal planes, respectively. The predominance of (111) and (200) peaks indicates that the Ag nanoparticles have spherical shapes. Ag_2O and AgCl nanoparticles exhibited sharp peaks which were observed at angles of 32°, 34°, and 78°. Each crystallographic face contains energetically distinct sites based on the atom density.

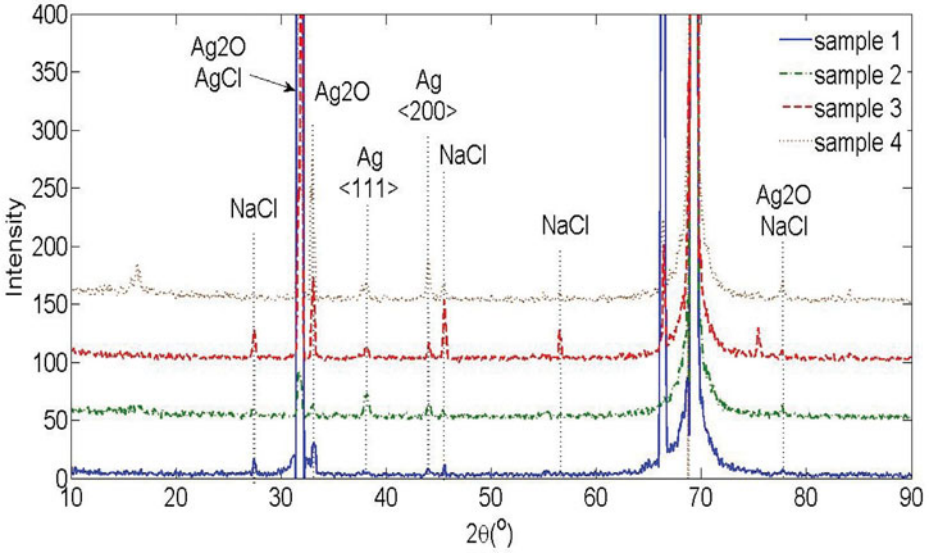

Figure 2. X-ray diffraction pattern of Ag nanoparticle samples after drying.

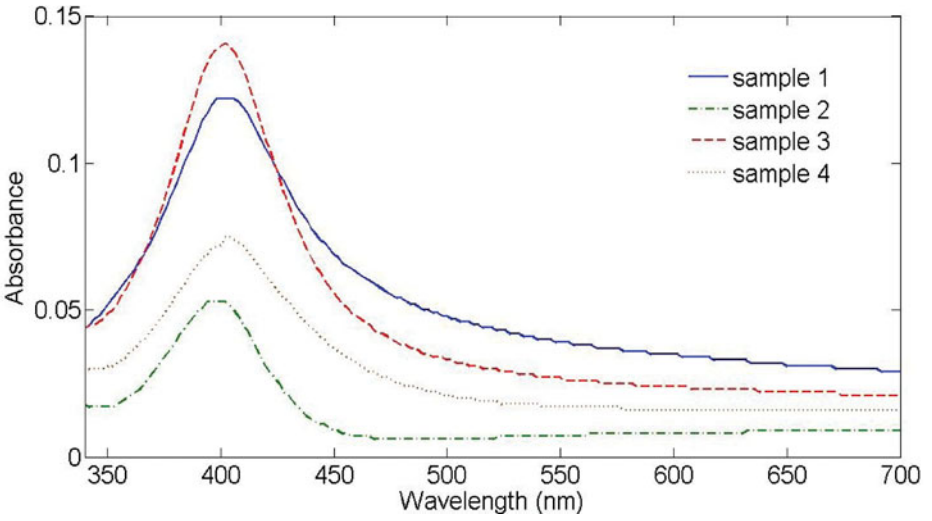

Figure 3. UV–Vis–NIR absorption spectrum of Ag nanoparticles in distilled water and distilled water with three different concentrations of NaCl.

Absorption spectrums of nanoparticle solutions are presented in Fig. 3. The absorbance of suspended Ag nanoparticles prepared by PLA in distilled water and distilled water with three different concentrations of NaCl was measured in the 300–700 nm wavelength range with respect to distilled water and distilled water with three different concentrations of NaCl absorption as the baseline. Figure 1 presents the optical absorption spectra of Ag nanoparticle solutions. For different samples, this number is different in the experiment. They demonstrate a visible absorption peak from the SPR absorption of Ag nanoparticles at 398–404 nm. Shifts in the position of SPR peak may represent varying particle size. The shift toward longer wavelength (red shift) of the prepared nanoparticle thus indicates increased particle size [24]. Absorption spectra clearly showed that the particle size of silver nanoparticles, produced by 532 nm laser wavelength, increased on increasing the concentrations of NaCl. This phenomenon was also confirmed in the particle size distribution obtained from the TEM image. The comparison between the absorbance spectra of sample 1 and sample 2 does not show in a convincing manner a red shift in the position of the SPR peak. The shift is too small to be reliable for exhibiting the difference between the sizes of nanoparticles in suspensions. The difference in the shape of the plasmonic bands indicated the change in the shape of the nanoparticles, their aggregation, and the size distribution under different concentrations of NaCl [25]. From Fig. 3, it is found that smaller nanoparticles are also present in the samples 1–4.

Figure 4 present SEM images of Ag nanostructures prepared by laser ablation in distilled water and distilled water with three different concentrations of NaCl. Images are prepared with 20 keV electrons leading to 30 k× magnification. Nanoparticle solutions were dried on Al foil at room temperature before imaging. The morphology of Ag nanoparticles depends on concentrations of NaCl for distilled water. The generated grains of nanoparticles in this experimental condition are almost spherical and adhered to each other. This structure is similar to those reported in Ref. 23 prepared at room temperature. It is observable that with an increase in the concentration of NaCl for distilled water, the rate of adhesion is decreased and grains are smaller. Specially, in the case of s2, there is no grain form in

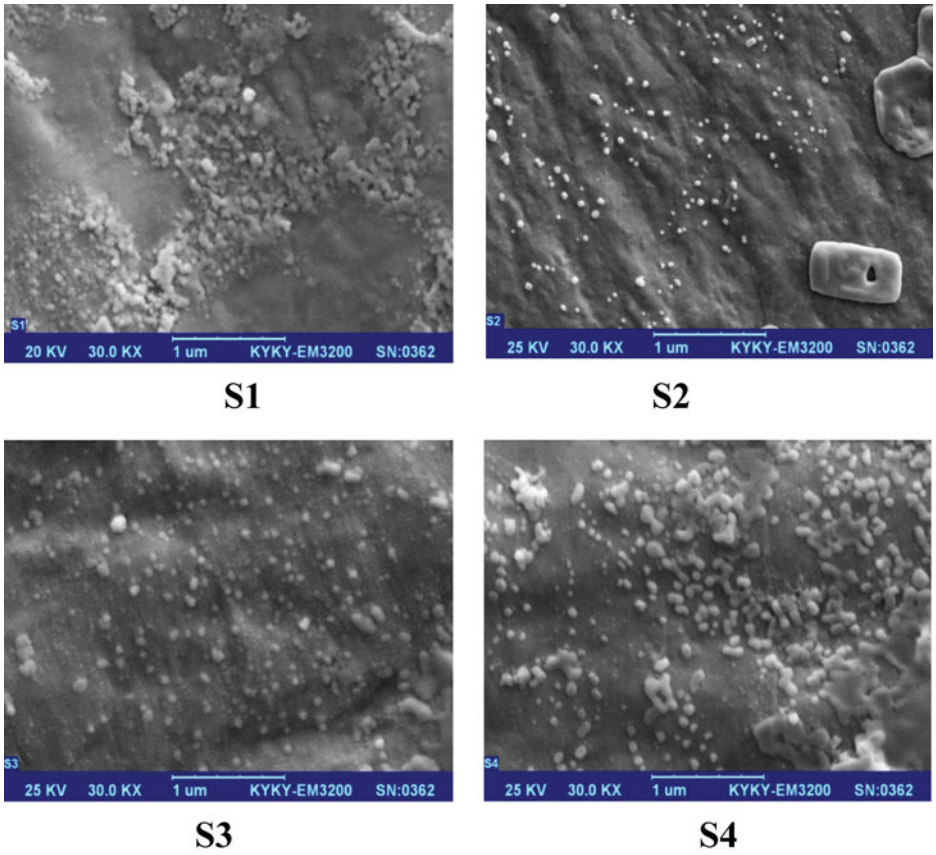

Figure 4. SEM micrographs of Ag nanoparticle samples dried on aluminum foil.

the nanoparticle solution. The size of Ag nanoparticles is increased with increasing the concentration of NaCl for distilled water.

More information about the size and morphology of Ag nanoparticles are presented in Fig. 5. In Fig. 5, the hydrodynamic size distribution of samples measured by DLS is shown. Hydrodynamic size of nanoparticles is their real diameter plus the diameter of the electrostatic potential around them, so it is larger than the real size of nanoparticles. According to the spectra obtained, the peak of hydrodynamic size distribution of samples for sample 1 is 24.6 nm, the peak of sample 2 occurrs at 5.6 nm and this size is decreased than sample 1. This peak of sample 3 was found to be increased and was measured at 19.1 nm. Finally, this peak of sample 4 decreased in the 18.6 nm range. The peak that occurred at larger size is due to ablated nanoparticles while the peak corresponding to smaller size is due to ablated nanoparticles which are fragments as per the concentration of NaCl for distilled water. With increase in the concentration of NaCl for distilled water in this regime of ablation, the size of nanoparticles is increased. For concentration of NaCl for distilled water of 5 mM and 15 mM, the secondary irradiation of nanoparticles by the concentration of NaCl has generated another class of smaller Ag nanoparticles.

TEM images of samples are presented in Fig. 6(a)–(e). In this set of images, the inter-grain structure can be observed. For TEM measurements, a drop of the solution containing

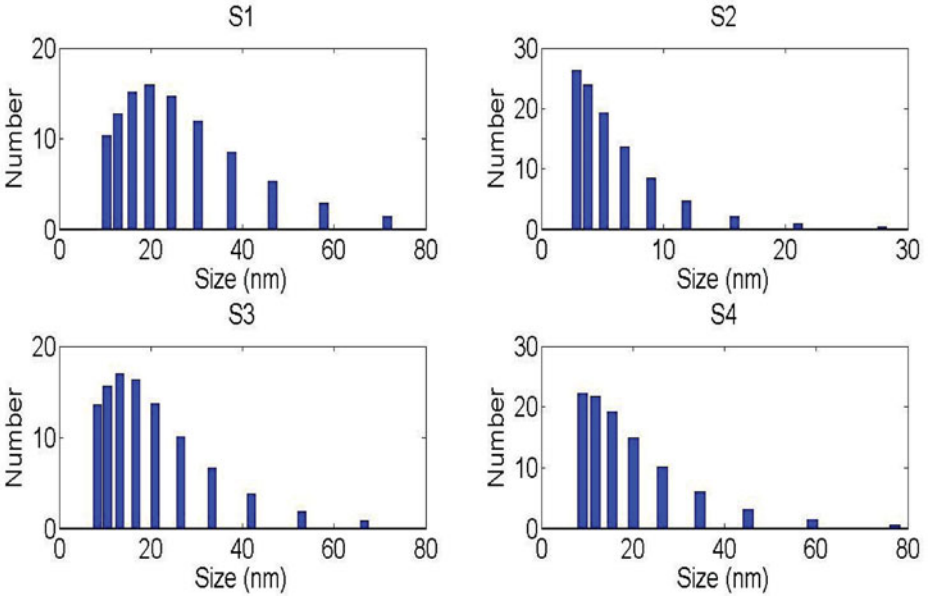

Figure 5. Ag nanoparticle hydrodynamic size distribution of samples measured by the DLS device.

nanoparticles is deposited and dried on a carbon-coated copper grid. Produced nanoparticles are spherical without any aggregation. The size distribution of nanoparticles can also be observed in Fig. 7. These graphs are plotted using the "measurement" software. We have a wide range of sizes of nanoparticles in each sample, but from samples 1–4, we can see that the peak of size distribution of samples tended to smaller values from 15 nm to 6 nm. The micrographs indicate that with an increase in NaCl concentration, the average size of the spherical nanoparticles increases. As can be seen, the silver nanoparticles are almost spherical in all the samples and the nanoparticle sizes and size distribution with increasing NaCl concentration therefore give rise to larger particles in samples 2, 3, and 4. This is therefore the solution to form colloidal nanoparticles in sample 1 that remain separated.

The average particle size obtained from DLS data were compared with the results obtained by TEM analysis. Considering that TEM and DLS analyses particle sizes differently, the results obtained from DLS and TEM can be considered to be in good agreement with each other. In both cases with increasing NaCl concentration, the size of nanoparticles is increased. But the size measured by the DLS device is larger than the sizes that can be observed in TEM micrographs. This difference can be due to the fact that DLS analysis includes the ligand shell and determines the hydrodynamic sizes of the synthesized nanoparticles whereas in TEM we can look at only the metallic core [23, 26].

In this work, photoluminescence properties of different silver nanoparticles in distilled water and distilled water with three different concentrations of NaCl have been investigated. The photoluminescence spectra from Ag nanoparticles are shown in Fig. 8. Photoluminescence emission spectra from the synthesized samples have been recorded at room temperature at 220 nm excitation wavelengths. The position and shape of the photoluminescence peak is almost independent of the excitation wavelength. Photoluminescence emissions spectra from the synthesized samples have been recorded at room temperature

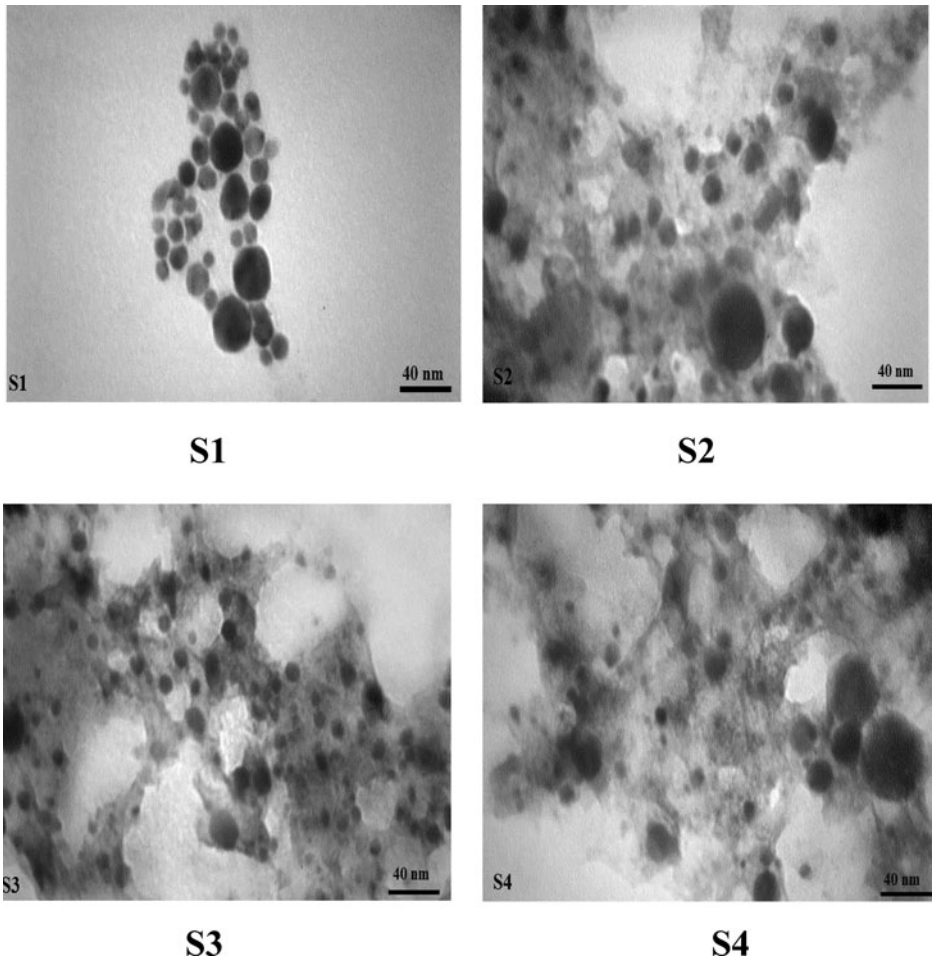

Figure 6. TEM image of Ag nanoparticles generated in NaCl solution with laser ablation mechanism.

at different excitation wavelengths. As can be seen in Fig. 8, the PL emission intensity increases with increasing NaCl concentration. The intensity of peaks may indicate intensive NaCl concentration due to the increase of interactions between nanoparticles due to higher concentration. It is found from Fig. 8 that samples exhibit PL emissions in the violet–blue and UV region. There is one intense peak in the photoluminescence of all samples which occurred in the range of 425 to 430 nm. This peak shows a red shift from sample 1 to 4. The schematic of the excitation and recombination mechanisms can be depicted as shown in Fig. 9, where the band structure for a typical noble metal is represented by a simple model. The band corresponding to 425–430 nm transition is observed only in the spectra of the samples containing the smallest Ag nanoparticles which are typically smaller than 10 nm and is absent in the samples with larger particles. This peak is very close to the peak of PL band of bulk silver [27–29]. This emission corresponds to the direct radiative interband recombination of the conduction sp-band electrons with holes in the valance d band that have been scattered to momentum states less that the Fermi momentum. The red shift of this peak may be due to coupling of these photons with SPR photons. The band

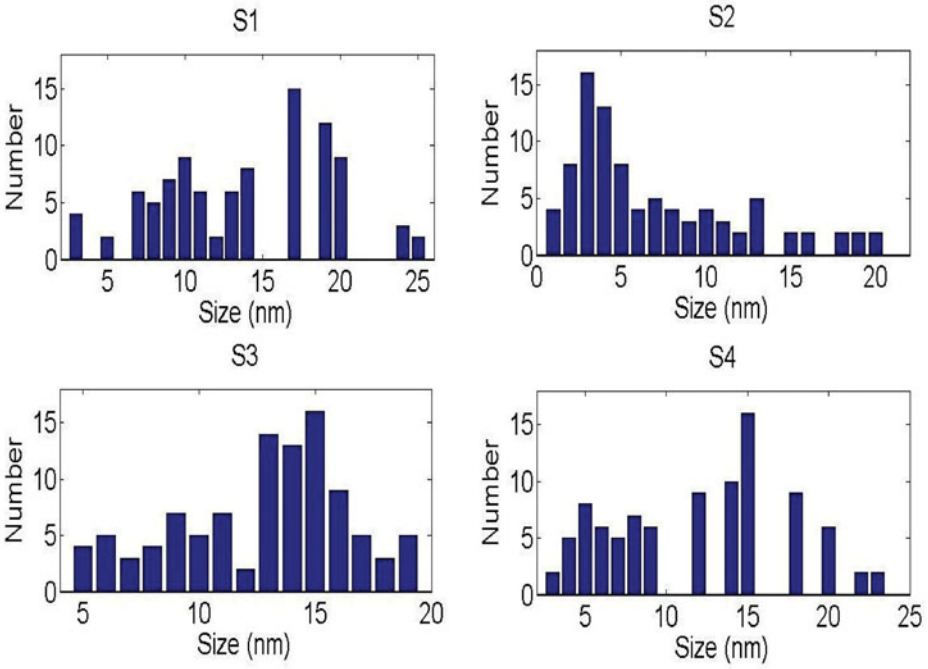

Figure 7. Particle size distribution of Ag nanoparticles generated in NaCl solutions with laser ablation mechanism.

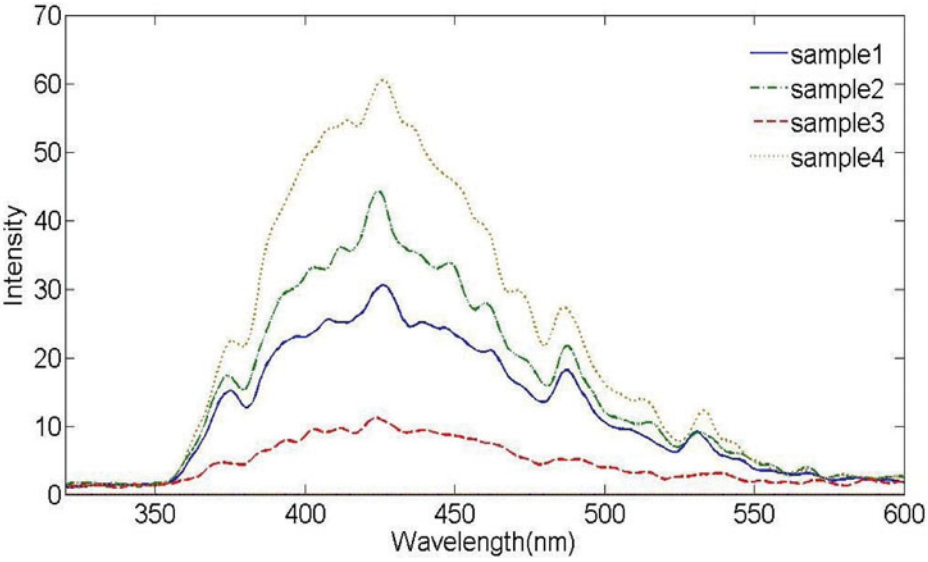

Figure 8. Photoluminescence spectra of Ag nanoparticles in NaCl solutions.

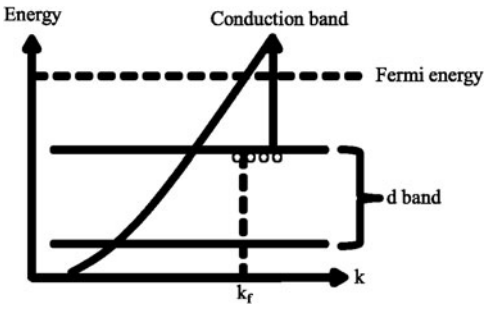

Figure 9. Excitation and recombination mechanism inside the band structure of noble metals.

corresponding to 425–430 nm is in the wavelength range of SPR excitation which is red shifted when the size of the particles increases. This behavior can be attributed to radiative decay of SPR excited in silver nanoparticles [30–32].

Peaks in the photoluminescence spectra nm 375, nm 425, nm 487, nm 535 correspond to equivalent energy 3.30 eV, 2.91 eV, 2.54 eV, and 2.32 eV, respectively. This peak, observed in all the samples, is likely to be the strongest peak that occurred at the peak of the optical band gap of 425 nm. And these represent peak levels of disturbance due to the formation of bands in the formation of nanoparticles.

Conclusions

Preparation of silver nanoparticles by laser ablation method in distilled water and distilled water with three different concentrations of NaCl is investigated. The generated nanoparticles in this experimental condition are spherical. The size of nanoparticles is increased by increasing the NaCl concentration and the rate of adhesion is decreased and grains are smaller. Absorption spectra show a clear and discrete absorption peak due to interband transitions along with the plasmon peak. The interband absorption dominates the plasmon absorption on increasing nanoparticle size. The peaks of X-ray diffraction patterns of nanoparticles can be indexed into the cubic phase of NaCl, Ag2O, AgCl, and Ag. The room temperature photoluminescence spectra of silver nanoparticles show that increasing the intensity of peaks may lead to intensive NaCl concentration due to the increase of interactions between nanoparticles. With increase in the NaCl concentration, a smaller class of nanoparticles is formed due to secondary interaction of laser pulse and ablated nanoparticles. The effect of this smaller class is clear in DLS hydrodynamic size distribution and PL spectrums.

References

[1] Scaffardi, L. B., Pellegri, N., de Sanctis, O., & Tocho, J. O. (2005). *Journal of nanotechnology*. *16*, 158–163.
[2] Patel, K., Kapoor, S., Dave, D. P., & Mukherjee, T. (2005). Synthesis of Nanosized Silver Colloids by Dielectric Heating. *J. Chem. Sci*. *117*(1), 5360.
[3] Henglein, A. (1993). *J. Phys. Chem.*, *97*, 5457.
[4] Toshima, N., Nakata, K., & Kitoh, H. (1997). *Inorg. Chim. Acta*, *265*, 149.
[5] Haruta, M. (1997). *Catalysis Today*, *36*, 153.
[6] Mirkin, C. A., & Letsinger, R. L. (1996). *Nature*, *382*, 607.
[7] Sonvico, F., Dubernet, C., Colombo, P., & Couvreur, P. (2005). *Curr. Pharm. Des.*, *11*, 2091.

[8] Mandel, S., Phadtare, S., & Sastry, M. (2005). *Curr. Appl. Phys.*, *5*, 118.
[9] Bieri, N. R., Chung, J., Haferi, S. E., Poulikakos, D., & Grigoropoulos, C. P. (2003). *Appl. Phys. Lett.*, *82*, 3529.
[10] Walter, E. C., Murray, B. J., Favier, F., & Penner, R. M. (2003). *Adv. Mater.*, *15*, 396.
[11] Watanabe, A., Kobayashi, Y., Konno, M., Yamada, S., & Miwa, T. (2005). *Jpn. J. Appl. Phys.*, *44*, L740.
[12] Smitha, S. L., Nissamudeen, K. M., Philip, D., & Gopchandran, K. G. (2008). *Spectrochimica Acta Part A*, *71*, 186.
[13] Durán, N., Marcarto, P. D., De Souza, G. I. H., Alves, O. L., & Esposito, E. (2007). *J. Biomed. Nanotechnol.*, *3*, 2.
[14] Barcikowski, S., Hahn, A., Kabashin, A. V., & Chichkov, B. N. (2007). *Appl. Phys.*, *87*, 47.
[15] Dorranian, D., Solati, E., & Dejam, L. (2012). *Appl. Phys. A*, *109*, 307.
[16] Cobley, C. M., Chen, J., Cho, E. C., Wang, L. V., & Xia, Y. (2011). Gold nanostructures: a class of multifunctional materials for biomedical applications. *Chemical Society Reviews 40*(1), 44–56.
[17] Vorobyova, S. A., Lesnikovich, A. I., & Sobal, N. S. (1999). Preparation of Silver Nanoparticles by Interphase Reduction. *Colloids Surf. A*, *152*, 375.
[18] Choi, S. H., Zhang, Y. P., Gopalan, A., Lee, K. P., & Kang, H. D. (2005). Preparation of Catalytically Efficient Precious Metallic Colloids by γ-Irradiation and Characterization. *Colloids Surf. A*, *256*, 165.
[19] Li, Z., Li, Y., Qian, X. F., Yin, J., & Zhu, Z. K. (2005). A Simple Method for Selective Immobilization of Silver Nanoparticles. *Appl. Surf. Sci.*, *250*, 109. Link, S., & EL-Sayed, M. A.(2000). *Int. Rev. Phys. Chem.*, *19*, 3.
[20] Tsuji, T., Watanabe, N., & Tsuji, M. (2003). Laser Induced Morphology Change of Silver Colloids: Formation of Nano-size Wires. *Appl. Surf. Sci.*, *211*, 189.
[21] Li, B., Kawakami, T., & Hiramatsu, M. (2003). *Appl. Surf. Sci.*, *210*, 171.
[22] Dorranian, D., Solati, E., & Dejam, L. (2012). *Appl. Phys. A*, *109*, 307.
[23] Lee, M. T., Hwang, D. J., Greif, R., & Grigoropoulos, C. P. (2009). *Int. J. Hydrog. Energy*, *34*, 1835.
[24] Yang, G.-W., Wang, J.-B., & Liu, Q.-X. (1998). *J. Phys.: Condens. Matter*, *10*, 7923.
[25] Wang, J.-B., & Yang, G.-W. (1999). *J. Phys.: Condens. Matter*, *11*, 7089.
[26] Fayaz, M., Tiwary, C. S., Kalaichelvan, P. T., & Venkatesan, R. (2010). *Colloids Surf. B*, *75*, 175.
[27] Yeshchenko, A. *et al.* (2009). *Phys. Rev. B*, *79*, 235438.
[28] Apell, P., Monreal, R., & Lundqvist, S. (1988). *Phys. Scr.*, *38*, 174.
[29] Whittle, D. J., & Burstein, E. (1981). *Bull. Am. Phys. Soc.*, *26*, 777.
[30] Zhang, A. P., Zhang, J. Z., & Fang, Y. (2008). *J. Lumin.*, *128*, 1635.
[31] Basak, D., Karan, S., & Mallik, B. (2006). *Chem. Phys. Lett.*, *420*, 115.
[32] Akimov, A. V. *et al.* (2007). *Nature _London*, *450*, 402.